Surfaces and Interfaces 26 (2021) 101427

Contents lists available at ScienceDirect

Surfaces and Interfaces

journal homepage: www.sciencedirect.com/journal/surfaces-and-interfaces

Understanding alloying behaviors of Sc, Ni and Zn additions on Al/TiB_2 interfaces based on interfacial characteristics and solute properties

Qian Wang [a,b], Yuanyuan Li [a,b], Zhe Chen [b], Mingliang Wang [a,*], Hong Zhu [b,c,*], Haowei Wang [a,b]

[a] State Key Laboratory of Metal Matrix Composites, Shanghai Jiao Tong University, Shanghai 200240, China
[b] School of Materials Science and Engineering, Shanghai Jiao Tong University, Shanghai 200240, China
[c] University of Michigan - Shanghai Jiao Tong University Joint Institute, Shanghai Jiao Tong University, Shanghai 200240, China

ARTICLE INFO

Keywords:
First-principles study
Al/TiB_2 interface
Alloying mechanisms
Interface orientation
Solute properties

ABSTRACT

In this study, the alloying effects of Sc, Ni and Zn elements on both Al(001)/TiB_2(0001) and Al(111)/TiB_2(0001) interfaces were assessed using first-principles calculations. The most thermodynamically stable Al/TiB_2 interface models with Ti terminal and center stacking sequences were selected. To describe interfacial stability and wettability, the interface energy and the work of adhesion were calculated, respectively. For interfacial stability, the alloyed Al(001)/TiB_2(0001) interfaces followed the sequence of Ni > Zn > Sc, while an inverse order was found on the alloyed Al(111)/TiB_2(0001) interfaces. For interfacial wettability, Sc- and Ni-alloyed Al(111)/TiB_2(0001) interfaces displayed an obvious improvement, and the others showed a slight change. The analysis results of chemical bonding and strain distribution illustrated that the alloying effect of Sc and Ni addition mainly relied on the interfacial structure, and the Zn doping interface largely depended on atomic properties. Consequently, the alloying behavior of solute atoms on the Al/TiB_2 interface can be explained by the atomic size effect and electronic interaction.

1. Introduction

Metal/ceramic interfaces play a key role in a wide range of technological applications such as anti-corrosion coatings, heterogeneous catalysis, electric devices, and structural components [1,2]. In ceramic-reinforced metal matrix composites (MMCs), interfacial wettability has an important influence on the final mechanical behavior of the composites [3,4]. To enhance interfacial wettability, alloying is an effective method [5,6]. For example, the addition of a small number of reactive metals (i.e., Mg, Ti, Zr) into some MMCs (e.g., Al/SiC, Ag/ZrB_2, Al/TiB_2) can increase their stability and wettability [7–10]. In our previous work, the addition of eleven alloying elements (i.e., Mg, Ca, Ag, Ce, Au, Pd, Y, Sc, Pt, Hf, and Zr) can enhance the interfacial stability and wettability of the Al(111)/TiB_2(0001) interface to promote the dispersion of TiB_2 particles in Al matrix [11]. However, some useful alloying elements for Al/TiB_2 system used in the experiment are absent from the above-mentioned elements. For example, Wang et al. reported that Zn addition improved the TiB_2 dispersion in the Al matrix [12,13]. Xi et al. found that the interfacial wettability between liquid Al and TiB_2 ceramics is augmented by Ni participation [14,15]. The key role of these improvements is mainly due to the enhancement of interfacial stability and wettability between TiB_2 and Al [16–18]. Nevertheless, the alloying effects of these elements (i.e., Ni and Zn) can hardly be reflected on the Al(111)/TiB_2(0001) interface. Thus, further exploration should be required.

Generally, the alloying effects of solute atoms on the interface depend on the properties of solute atoms (i.e., valence electron density, atomic radius, and so on) [19–23] and interface structure [24–27]. For example, Tsuru et al. illustrated that the influence of solute elements on interfacial segregation and fracture in Mg twin boundaries was affected by the electron interaction [28]. Shin et al. showed that the segregation energies of 34 elements in the Al/Al_2Cu interface are strongly correlated with the size and volume of solute atoms and their solubilities within the Al_2Cu phase [29]. Moreover, AlMotasem et al. reported the opposite segregation behavior of Ti and Ta elements at six different symmetric tilted grain boundaries of W due to the lattice distortion and electronic contribution [27]. Wang et al. found that the interface energy of the Fe (111)/Cu(111) interface was reduced larger than Fe (110)/Cu(110) interface with Ni addition [24].

Furthermore, it is noteworthy that the importance of the above-mentioned influence factors may vary for different solute atoms at certain interfaces. For instance, He et al. found that the alloying

* Corresponding authors.
E-mail addresses: mingliang_wang@sjtu.edu.cn (M. Wang), hong.zhu@sjtu.edu.cn (H. Zhu).

https://doi.org/10.1016/j.surfin.2021.101427
Received 5 July 2021; Received in revised form 12 August 2021; Accepted 25 August 2021
Available online 4 September 2021

behavior of Bi, Pb, Tl, and In elements on the coherent twin boundaries of Mg was mainly dominated by the chemical bonding [21], and the Gd and Zn atoms mostly depended on the elastic strain minimization [30]. Therefore, the analysis of alloying behavior of various solute atoms on the interface should be based on both solute properties and interfacial orientations.

For Al/TiB_2 composites, there are two common interface orientations (i.e., Al(111)/TiB_2(0001) and Al(001)/TiB_2(0001)) observed in the experiments [31–33]. The previously theoretical works mainly focused on the Al(111)/TiB_2(0001) interface [34–37], which may be not comprehensive. For instance, our previous calculation results showed that the addition of Ni (Zn) exhibited a negative (weak) influence on the interfacial stability and wettability of Al(111)/TiB_2(0001) interface [11], which was ever consistent with the experimental phenomenon [12–15]. Thus, a further investigation of the influence of Ni and Zn additions on the Al(001)/TiB_2(0001) interface is necessary. Moreover, the previous study showed that the addition of low *d* elements (i. e., Sc, Y, Zr, Ce, Hf) shows the optimum improvement on the stability and wettability of the Al(111)/TiB_2(0001) interface, but their influence on the Al (001)/TiB_2(0001) interface has been rarely reported. Hence, the typically Sc element is selected to explore the alloying mechanism on the Al (001)/TiB_2(0001) interface.

Based on the above discussion, the objective of this work is twofold. (1) The alloying effects of Sc, Ni, and Zn on both Al(001)/TiB_2(0001) and Al(111)/TiB_2(0001) interfaces were investigated via first-principles calculation. The interfacial stability and wettability of the initial and alloyed interfaces were systematically investigated by the calculated interface energy and work of adhesion. (2) The alloying mechanism on both Al/TiB_2 interfaces was explored. The chemical bonding and strain distribution were comprehensively analyzed by the charge density difference and Voronoi volume. Our calculations can provide a guide to alloying design of such metal/ceramic interfaces.

2. Computational details

The DFT calculations were performed in the Vienna Ab initio Simulation Package (VASP) with the projected augmented wave (PAW) pseudopotentials and a plane-wave basis set [38]. The Perdew-Burke-Ernzerhof (PBE) exchange-correlation functional within the generalized gradient approximation (GGA) was applied [39–41]. A plane wave cut-off of 450 eV was set with 10^{-5} eV/atom energy convergence parameter for the electronic self-consistent part. The maximum forces on each relaxed atom were converged to 0.02 eV/Å during structural relaxation via conjugate gradient minimization. The valence electrons for the adopted pseudopotentials of Al, B, and Ti atoms were $3s^2 3p^1$, $2s^2 2p^1$ and $3s^2 3p^6 3d^2 4s^2$, respectively. The mesh of Γ-centered *k*-points to sample the Brillouin zone was chosen and their density was less than 0.03 $Å^{-1}$. During the geometry optimization, both the volume and atomic positions were relaxed for the initial interface systems, and only the atomic positions of the alloyed interface systems were relaxed.

3. Results and discussion

3.1. Initial Al /TiB_2 interfaces

Based on the experimental characterization [31–33], there are two interface orientation relationships (i.e., Al(111)/TiB_2(0001) and Al (001)/TiB_2(0001)) identified in Al/TiB_2 composite. For Al (111)/TiB_2(0001) interface, the available calculated results showed that the interface with Ti-terminal and center stacking sequence was the most stable interface model [11,34,36]. However, for Al (001)/TiB_2(0001) interface, there is still a lack of theoretical research on its interfacial structure characterization. Hence, the stability of the Al (001)/TiB_2(0001) interface model is investigated for the first time.

3.1.1. Structure construction of Al(001)/TiB_2(0001) interface

Based on the convergence test (Section S1 in Supplementary Materials), six-layer Al(001) slabs and nine-layer Ti- or B-terminated TiB_2(0001) slabs were used to construct Al(001)/TiB_2(0001) interface supercell models. According to the planar lattice parameters and interface orientation (Table 1), a $1 \times \sqrt{3}R30^\circ$ TiB_2(0001) surface slab is placed between two 1×2 Al(001) surface slabs to build an Al(001)/TiB_2(0001) interface supercell model. The lattice misfit (δ) on the interface was defined as $\delta = 2 \times (b_{Al} - b_{TiB_2})/(b_{Al} + b_{TiB_2}) \times 100\ \%$ [42,43].

Four different interface models were constructed by considering the termination (Ti or B) and interfacial stacking sequence (i.e., center and top). These models are presented in Fig. 1a, where the locations of Al atoms are different. Taking Ti terminal models as an example, in the center stacking sequence, the interfacial Al atoms are located above the B atoms of the TiB_2(0001) subsurface. In the top stacking, the interfacial Al atoms are located above the surface Ti atoms of the TiB_2(0001) slab.

To obtain the initial interfacial distance (d_0) of these Al(001)/TiB_2(0001) interface models, the work of adhesion (W_{ad}) of the unrelaxed interfacial structure [44,45] was calculated using the following equation [10,46]:

$$W_{ad} = \frac{1}{2A}\left(E_{slab}^{Al} + E_{slab}^{TiB_2} - E_{interface}\right) \quad (1)$$

where, E_{slab}^{Al} and $E_{slab}^{TiB_2}$ are the total energy of a six-layer Al(001) surface and a nine-layer TiB_2(0001) surface with the same lattice parameters of their interface models, respectively.

$E_{interface}$ represents the total energy of the fully relaxed interface model.

2A stands for the total area of two interface regions in each interface model (i.e. two identical interfaces at both top and bottom of the model).

The work of adhesion is calculated by changing the separation distance, which is between two rigid free surfaces from 1.5 to 4 Å. In Fig. 1b, the Ti-center interface has the highest W_{ad} at d_0=2.20 Å. Thus, the initial interface distance (d_0) is set to 2.20 Å. Similarly, the initial interfacial distances for Ti-top, B-top, and B-center interface models are set to 2.50 Å, 2.00 Å, and 2.00 Å, accordingly (Fig. 1b). After the interface structure is relaxed, the position of interfacial atoms is exhibited in Fig. 1a.

3.1.2. Interface stability of Al(001)/TiB_2(0001) interfaces

To investigate their interfacial bonding strength and interface stability, the interfacial distance (d_0) and the work of adhesion (W_{ad}) of the relaxed Al(001)/TiB_2(0001) interface are calculated and listed in Table 2. After relaxation, for Ti-terminated interface models, the Ti-center interface structure is much more stable than the Ti-top interface because of its smaller d_0 and the larger W_{ad}. For the B-terminated interface models, the B-center and B-top interfaces exhibit similar values of d_0 and W_{ad} in Table 2. This can be explained by the B-top interface model changed to the B-center interface structure via relaxation (Fig. 1a). Thus, the B-center interface structure is the most stable case. In addition, the Ti-center Al(001)/TiB_2(0001) interface has a higher W_{ad} value than B-center. Therefore, the Ti-center interface shows a higher interfacial bonding strength.

The interface stability of the Al(001)/TiB_2(0001) interface is further evaluated based on the interface energy from the thermodynamic

Table 1.
Planar lattice parameters and orientations of Al and TiB_2 slabs employed for Al (001)/TiB_2(0001) interfaces.

Model	*a* (Å)	*b* (Å)	*θ* (°)	δ
Al slab	2.86	5.73	90	-
TiB_2 slab	3.03	5.25	90	-
Interface	3.03	5.25	90	8.27%

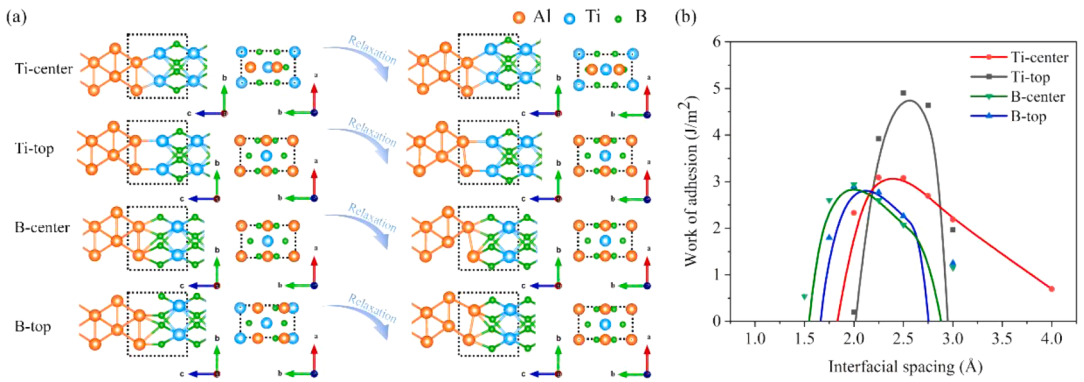

Fig. 1. (a) Different interfacial stacking sequences of Ti and B-terminated Al(001)/TiB_2(0001) interface models at both unrelaxed and relaxed states. (b) Work of adhesion as a function of the unrelaxed interfacial distance for Ti and B-terminated Al(001)/TiB_2(0001) interface structure with two stacking sites.

Table 2.
Interfacial spacing (d_0) and the work of adhesion (W_{ad}) of Al(001)/TiB_2(0001) interface models.

Interface model(Terminal-Stacking sequence)	Unrelaxed d_0 (Å)	Relaxed d_0 (Å)	W_{ad} (J/m^2)
Ti-center	2.20	2.25	3.59
Ti-top	2.50	2.49	2.67
B-center	2.00	1.85	3.49
B-top	2.00	1.85	3.48

viewpoint. The interface energy (γ_{int}) is defined as follows [47,48]:

$$\gamma_{int} = \frac{1}{2A}\left(E_{interface} - N_{Al}\mu_{Al} - N_{Ti}\mu_{Ti} - N_B\mu_B\right) \quad (3)$$

where N_{Al}, N_{Ti}, and N_B refer to the number of the Al, Ti, and B atoms in the interfaces, accordingly.

μ_{Al}, μ_{Ti}, and μ_B are the chemical potentials of corresponding atoms, accordingly. In our calculation, μ_{Al} refers to the energy of bulk FCC Al per atom. μ_{Ti} and μ_B are related to each other by the existence of the TiB_2 bulk phase [49].

Therefore, the interface energies of Ti-center and B-center Al(001)/TiB_2(0001) interfaces can be plotted as a function of the chemical potential of B (Fig. 2). As the chemical potential of B increases, the interface energy of the B-center interface decreases, and that of the Ti-center interface increases. In detail, the Ti-center interface shows smaller interface energy (0.39 J/m^2) at the Ti-rich condition. For the B-rich case, the smaller interfacial energy is assigned to the B-center interface (1.49 J/m^2). Over most of B chemical potential, the Ti-center interface has smaller interface energy, which is thermodynamically more favorable.

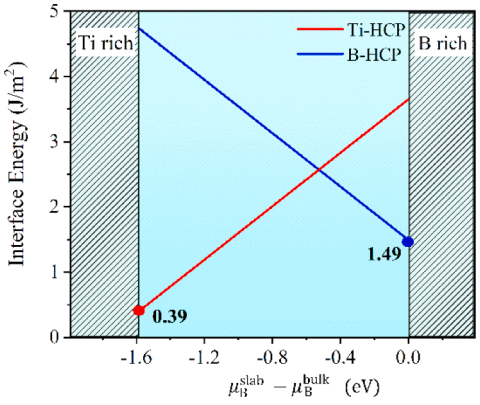

Fig. 2. Calculated Al(001)/TiB_2(0001) interfacial energies as a function of the chemical potential of B.

Combined with the work of adhesion (Table 2), it can be found the Ti-center interface model is the most thermodynamic stable case.

Accordingly, the interfacial Al atoms prefer to obey the center stacking sequence of the TiB_2 surface with Ti or B termination. A similar phenomenon can be observed on the Al(111)/TiB_2(0001) interface [11,34,36]. As a result, the Ti-center interface model has the highest thermodynamic stability in both Al(001)/TiB_2(0001) interface and Al(111)/TiB_2(0001) interface. Therefore, it is applied to further study the alloying effects on these interface characteristics.

3.2. Alloyed Al/TiB_2 interfaces

3.2.1. Interfacial stability of alloyed interfaces

To conduct a comprehensive study of alloying design, the alloying ratio was set to 2 at% [11]. It means that one alloying atom X (i.e., Sc, Ni, Zn) was introduced into each interface of a 2 × 1 × 1 Ti-center Al(001)/TiB_2(0001) interface supercell (Fig. 3a) and a 2 × 2 × 1 Ti-center Al(111)/TiB_2(0001) interface supercell (Fig. 3b). After comparing the different doping methods (Section S2 in Supplementary Materials), three substitution sites (Al_i, Al_{i-1}, Al_{i-2}) from the interface to the bulk region were selected to determine the optimal substitution position of the alloying atom. To evaluate the site preference of the alloying atoms and the stability of the alloyed interface, the relative interface energy ($\Delta\gamma_{int}$) was calculated using the following formula [50–55]:

$$\Delta\gamma_{int} = \frac{1}{2A}\left[\left(E^{x}_{interface} - E_{interface}\right) - NX\left(\mu^{bulk}_{X} - \mu^{bulk}_{Al}\right)\right] \quad (5)$$

where $\Delta\gamma_{int}$ is the relative interface energy of the alloyed interface. A negative value of $\Delta\gamma_{int}$ indicates that the alloying atom (X) can enhance interfacial thermodynamic stability by reducing the interface energy.

$E_{interface}$ ($E^{X}_{interface}$) is the total energy of the initial (alloyed) interface supercell.

N_X is the number of alloyed atoms in the supercell.

To calculate the μ^{bulk}_{X}, a bulk model with 24 Al atoms is applied, and the central Al atom is replaced by an X atom.

After introducing the alloying atoms X into the interface supercell, the $\Delta\gamma_{int}$ values of alloyed Al(001)/TiB_2(0001) and Al(111)/TiB_2(0001) interfaces were calculated and displayed in Fig. 3a and b, respectively. Since the alloying atoms are replaced at three different positions from the interface to the bulk region, each alloy element forms three different doping interfaces. To facilitate the study, they are simplified to Al_i, Al_{i-1}, and Al_{i-2} interfaces in the following discussion.

For Sc-alloyed Al(001)/TiB_2(0001) interfaces (Fig. 3a), three different doping interfaces all have positive $\Delta\gamma_{int}$ values, which means that the Sc addition weakens the interface stability. Furthermore, compared with the Al_i (0.75 J/m^2) and Al_{i-1} (0.23 J/m^2) interfaces, it can be found that the Al_{i-2} interface has the lowest $\Delta\gamma_{int}$ value (0.20 J/m^2), indicating that the optimal substitution location for the Sc atom

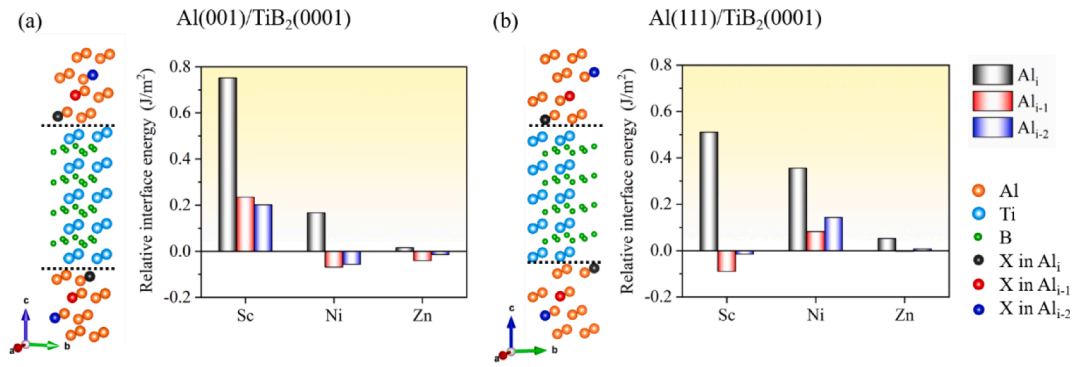

Fig. 3.. Schematic diagram of atomic substitution sites of alloying elements and relative interface energies of Sc-, Ni- and Zn-alloyed interfaces. (a) Ti-center Al (001)/TiB_2 (0001) interface supercells, (b) Ti-center Al (111)/TiB_2 (0001) interface supercells [11]. The interface energy of the initial interface is set to zero.

belongs to the Al_{i-2} position. For Ni-doping Al(001)/TiB_2(0001) interfaces, the $\Delta\gamma_{int}$ value of the Al_i interface is positive (0.15 J/m^2). However, the $\Delta\gamma_{int}$ values of Al_{i-1} and Al_{i-2} interfaces are both negative. Moreover, the Al_{i-1} interface (-0.07 J/m^2) has a lower $\Delta\gamma_{int}$ value than that of the Al_{i-2} interface (-0.06 J/m^2). Thus, the ideal replacement location of the Ni atom is the Al_{i-1} site. For Zn alloyed Al(001)/TiB_2(0001) interfaces, the difference of interface energy on the three types of doping interfaces is small. Compared with the Al_i (0.02 J/m^2) and Al_{i-2} (-0.01 J/m^2) interfaces, the $\Delta\gamma_{int}$ value obtains the minimum at the Al_{i-1} interface (-0.03 J/m^2). Hence, the optimal substitute position of the Zn atom is the Al_{i-1} site.

For Sc-alloyed Al(111)/TiB_2(0001) interfaces (Fig. 3b), when the Sc atom is introduced in the Al_i site, the $\Delta\gamma_{int}$ value obtains the maximum value (0.51 J/m^2). If the Sc atom is doped at the Al_{i-1} site, the $\Delta\gamma_{int}$ value obtains the minimum value (-0.09 J/m^2). Hence, the ideal substituted position of the Sc atom is the Al_{i-1} site. For Ni-alloyed Al(111)/TiB_2(0001) interfaces, three types of doping interfaces all have positive $\Delta\gamma_{int}$ values. It means that the interface stability is weakened by the Ni addition. Furthermore, comparing the Al_i (0.36 J/m^2) and Al_{i-2} (0.14 J/m^2) interfaces, the Al_{i-1} interface obtains the minimum $\Delta\gamma_{int}$ value (0.08 J/m^2). Hence, the best substitution location for the Ni atom belongs to the Al_{i-1} site. For the Zn-alloyed Al(111)/TiB_2(0001) interfaces, the interface energies of three types of doping interfaces all display plaint changes. Moreover, only the Al_{i-1} interface has a slightly negative $\Delta\gamma_{int}$ value (-0.003 J/m^2), which is lower than the Al_i (0.05 J/m^2) and Al_{i-2} (0.007 J/m^2) interface. Thus, the optimal substitute position of Zn atom is the Al_{i-1} site.

Accordingly, the optimal substituted position for alloying atoms is mainly located at the Al_{i-1} site, except for the Sc-alloyed Al(001)/TiB_2(0001) interface (Al_{i-2} site). Considering that the energy difference between the Al_{i-1} and Al_{i-2} interfaces is about 1.12 ~ 4.84 % (Section S3 in Supplementary Materials), the Al_{i-1} position will be selected in subsequent studies to avoid the influence of the substitution position for the Sc atom. Moreover, comparing with the initial interface, the Sc introduction weakens the interfacial stability of Al(001)/TiB_2(0001) interface, while enhances that of the Al(111)/TiB_2(0001) interface. However, the Ni addition exhibits a converse effect. After Zn alloying, the interfacial stability for Al(001)/TiB_2(0001) interface is obviously enhanced, and Zn addition shows slight improvement on the Al(111)/TiB_2(0001) interface.

Consequently, the interface stability for the alloyed Al(001)/TiB_2(0001) interfaces obeys the sequence of Ni > Zn > Sc, and it changes to the order of Sc > Zn > Ni for the alloyed Al(111)/TiB_2(0001) interface. Considering that all alloying atoms are substituted at the Al_{i-1} site, the opposite alloying effects on the interfacial stability may be caused by different interface structures. To further explore the influence of interface orientation, the alloying effects on interface wettability are compared in the following section.

3.2.2. *Interfacial wettability of alloyed interfaces*

The work of adhesion (W_{ad}) of the optimal alloyed Al(001)/TiB_2(0001) and Al (111)/TiB_2(0001) interfaces is calculated to verify the role of alloying elements on the interfacial wettability and displayed in Fig. 4.

For the initial interface, the W_{ad} value of the Al(001)/TiB_2(0001) interface (3.59 J/m^2) is lower than that of the Al(111)/TiB_2(0001) interface (3.81 J/m^2). It is mainly because the lattice misfit (δ) on the interfaceof the former (8.27%) [34] is lower than that of the latter (5.75%). For the addition of Sc atoms, the alloying effects on both types of interfaces are different. The Sc-alloyed Al(001)/TiB_2(0001) interface has a lower W_{ad} value (3.56 J/m^2) than the initial interface (3.59 J/m^2), and the opposite tendency is displayed on the Sc-alloyed Al (111)/TiB_2(0001) interface (i.e., 4.03 J/m^2 for Sc-alloyed interface, 3.81 J/m^2 for initial interface). This may be caused by the different interface structures [25,56].

For the introduction of Ni atoms, the alloying effects exhibit a positive influence on both the Al(001)/TiB_2(0001) (3.60 J/m^2) and Al (111)/TiB_2(0001) interfaces (3.93 J/m^2). Compared with the initial interface, the enhanced degree of the former interface (0.01 J/m^2) is smaller than the latter interface (0.12 J/m^2), which is also due to the different interface structures. However, the alloying effects on both interfacial types are identical after adding the Zn atom. The W_{ad} value of the Zn-alloyed Al(001)/TiB_2(0001) interface is 3.62 J/m^2, which is slightly higher (0.03 J/m^2) than the corresponding initial interface. The same enhancement is shown in the Al(111)/TiB_2(0001) interface (i.e., 3.84 J/m^2 for the Zn-alloyed interface, 3.81 J/m^2 for the initial interface), which may be owing to the similar atomic radius and valence electron concentration between Al and Zn atoms (Table S4) [20,57].

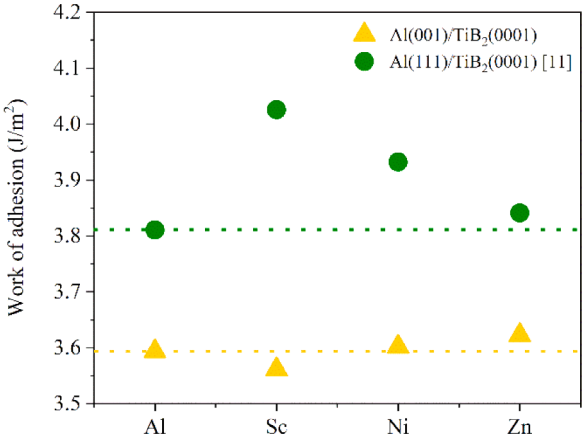

Fig. 4. Work of adhesion of Ti-center Al(001)/TiB_2(0001) and Al(111)/TiB_2(0001) interfaces without and with alloying atoms. The dotted line represents the initial interface.

Therefore, the interfacial wettability of the alloying Al(001)/TiB_2(0001) interfaces follows the sequence of Zn > Ni > Sc, and it obeys an opposite tendency on the Al(111)/TiB_2(0001) interface (i.e., Sc > Ni > Zn). Meanwhile, it is noteworthy that the interfacial wettability of Sc- and Ni-alloyed Al(111)/TiB_2(0001) interfaces has an obvious improvement, while that of the others displays a weak change. Considering the same substitution position of alloying atoms in both interfaces, the above-mentioned different alloying effects should be caused by different interface environments (i.e., interface structure, interface charge density, interface strain energy, and so on) [22,28,58]. The detailed mechanisms are discussed in the next section.

3.3. Alloying mechanism

The alloying effects of Sc, Ni, and Zn on both Al(001)/TiB_2(0001) and Al(111)/TiB_2(0001) interfaces are different by the analyses on the interface energy and work of adhesion. Considering the difference in atomic properties of these alloying elements (Section S4 in Supplementary Materials), the chemical bonding and strain distribution of the initial and alloyed Al/TiB_2 interfaces are discussed by the charge density difference and Voronoi volume to clarify the alloying mechanism.

3.3.1. Charge density difference

To provide a direct bonding description of atoms at the interface, the charge density difference maps of initial and alloyed Al/TiB_2 interfaces are calculated as follows [21,44,59]

$$\Delta\rho = \rho_{sc} - \rho_{atom} \tag{8}$$

where ρ_{sc} is the self-consistent charge density;

ρ_{atom} is the non-self-consistent charge density, i.e., the superposition of atomic charge densities.

The three-dimensional charge-density difference maps of the initial and alloyed Ti-center Al(001)/TiB_2(0001) interfaces are shown in Fig. 5a-d. To further clarify the alloying mechanisms of Sc, Ni, and Zn elements, the charge density difference maps of the Ti-center Al(111)/TiB_2(0001) interfaces are displayed in Figs. 5e-h. Meanwhile, the layer Projected Density of the State (PDOS) [60–62] of Al, Ti, and alloying atoms on these interfaces are calculated and plotted in Section S5 in Supplementary Materials to better understand the reason for charge density changes.

For the initial Al(001)/TiB_2(0001) interface (Fig. 5a), there are two types of charge accumulations (i.e., the Al-Ti and the Al-Al covalent bonds shown in Fig. S2a) which mainly appear on the interfacial layer (shown by the dotted line). Moreover, the charge accumulations of the Al-Ti bond in this interface are lower than that in the Ti-center Al(111)/TiB_2(0001) interfaces (Figs. 5e and S3a). This can be attributed to the low work of adhesion of the Al(001)/TiB_2(0001) interface. (Fig. 4).

For the Sc-alloyed Al(001)/TiB_2(0001) interface (Fig. 5b), the charge accumulations on the inner Al layers (i.e, Al_i, Al_{i-1}, and Al_{i-2} layers) increase. Considering the electronegativity of the Sc (1.36) and Al (1.61) atoms [63], the enhancement of these charge accumulations is caused by the formation of Al-Sc covalent bond (Fig. S2b) [64,65]. Moreover, the charge accumulations on the interfacial layer (shown by the dotted line) are less than that in the initial interface (Fig. 5a), which is consistent with the decrease of the interfacial stability and wettability. However, when we attempted to assess the Sc-alloyed Al(111)/TiB_2(0001) interface, an opposite phenomenon is recorded (Figs. 5f and S3b). It may be due to the different interfacial charge distribution in both types of initial interfaces.

For the Ni-alloyed Al(001)/TiB_2(0001) interface (Fig. 5c), the charge accumulations on the inner Al layers increase. Referring to the electronegativity of Ni (1.91) and Al (1.61) atoms, there are plenty of electrons transferring from Al to Ni atoms to form the Al-Ni covalent bond (Fig. S2c) [63], which leads to the charge reduction of the Al atoms at the Al_{i-1} layer. Compared with the charge density distribution of the initial interface (Fig. 5a), the charge accumulations on the interfacial layer increase. Nevertheless, a converse effect appears on the Ni-alloyed Al(111)/TiB_2(0001) interface (Figs. 5g and S3c). Considering the charge distributions in both initial interfaces are different, the alloying effect of the Ni element on the Al/TiB_2 interface should be largely determined by the interface structure.

For the Zn-alloyed Al(001)/TiB_2(0001) interface (Fig. 5d), the charge density distribution is similar to the initial interface (Fig. 5a). This is owing to the analogous electronegativity of Zn (1.65) and Al (1.61) atoms and the similar valence electron concentration [19]. Therefore, the addition of Zn shows little effect on the interfacial stability (Fig. S2d). A similar alloying influence also exists in the Zn-alloyed Al(111)/TiB_2(0001) interface (Figs. 5h and S3d). Thus, the alloying effect of Zn addition mainly depends on the valence electron of the solute atom.

Accordingly, the converse alloying effects of Sc and Ni elements on the Al(001)/TiB_2(0001) and Al(111)/TiB_2(0001) interfaces are mainly owing to the different charge distribution of the initial interface. The consistent alloying effect of the Zn element on the Al/TiB_2 interfaces relies on the similar electronegativity between Zn and Al atoms. Therefore, the alloying effect on the Al/TiB_2 interfaces depends not only on the charge density distribution of the initial interface but also on the properties of the alloying atoms.

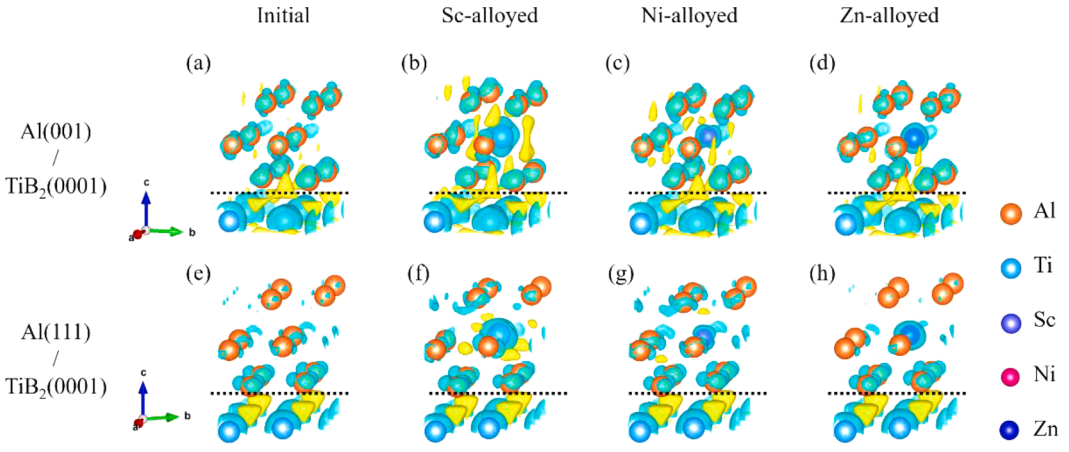

Fig. 5. Three-dimensional charge density differences maps of Ti-center Al (001)/TiB_2(0001) (a-d) and Al(111)/TiB_2(0001) interfaces (e-h) with an iso-surface value of 0.0065 e/Å^3: (a) and (e) initial interface, (b) and (f) Sc-alloyed interface, (c) and (g) Ni-alloyed interface, (d) and (f) Zn-alloyed interface. The yellow (blue) areas indicate electron accumulation (depletion), and the interfacial layer is indicated by a horizontal dotted line.

3.3.2. Voronoi volume

According to the change of charge density map, the alloying effects of Sc, Ni, and Zn elements are various. Moreover, the additions of Sc and Ni show an opposite alloying influence on both types of Al/TiB_2 interfaces. Considering the atomic radius differences of Al, Sc, Ni, and Zn atoms (Table S4), the interfacial strain distribution of the alloying interfaces is further discussed by Voronoi volume [28,66]. The Voronoi volume of the alloying atoms and nearby Al atoms (i.e., the atoms in Al_i, Al_{i-1}, and Al_{i-2} layers) are calculated via the VORO++ software [67]. The distribution maps of Voronoi volume of Al/TiB_2 interface are shown in Fig. 6, and the detailed information is listed in Section S6 in Supplementary Materials.

For the initial Al(001)/TiB_2(0001) interface (Fig. 6a), the Voronoi volume of the Al atoms at different layers obeys the order of $Al_i > Al_{i-1} > Al_{i-2}$ (Table S5). Comparing the Voronoi volume of the Al atoms in the bulk state (16.61 $Å^3$), the Al atoms at the Al_i layer are subjected to tensile strain, and the Al_{i-1} and Al_{i-2} layers are subjected to compressive strain. For the Sc-alloyed Al(001)/TiB_2(0001) interface (Fig. 6b), the Voronoi volume of the Sc atom substituted at the Al_{i-1} site is 16.71 $Å^3$, which is larger than the corresponding Al atom in the initial interface. Hence, a tensile strain should be inducted into the interface due to the larger atomic size of the Sc atom [30]. Moreover, after Sc alloying, the Voronoi volumes of Al atoms on the Al_i, Al_{i-1}, and Al_{i-2} layers increase by 0.06 $Å^3$, 0.30 $Å^3$ and 0.14 $Å^3$, respectively. Hence, the Sc addition causes the tensile strain inside the Al layers, which changes the strain distribution of the initial interface resulting in the decrease of both interfacial stability and wettability (Figs. 3a and 4).

Concerning the Ni-alloyed Al(001)/TiB_2(0001) interface (Fig. 6c), the Voronoi volume of the Ni atom is 15.15 $Å^3$. Accordingly, a compressive strain is added into the interface by the Ni atom with a smaller atomic size [28]. Furthermore, after Ni doping, the Voronoi volumes of Al atoms on the Al_i, Al_{i-1}, and Al_{i-2} layers decrease by -0.16 $Å^3$, -1.00 $Å^3$, and -0.27 $Å^3$, respectively. Hereby, the Ni substitution can release the compressive strain at the initial interface, which helps to improve the interfacial performance. For the Zn-alloyed Al (001)/TiB_2(0001) interface (.6d), the Voronoi volume of the Zn atom is 16.31 $Å^3$, which is similar to Al atoms in the initial interface. Besides, the variations of Voronoi volume of Al atoms on the inner Al layers are approximately zero (i.e, -0.01 $Å^3$ for the Al_i layer, -0.04 $Å^3$ for the Al_{i-1} layer, +0.02 $Å^3$ for the Al_{i-2} layer). Thus, Zn doping has a weak effect on the interfacial strain.

The strain distributions of Al(111)/TiB_2(0001) interfaces are different. For the initial interface (Fig. 6e), the Voronoi volume of the Al atoms at three-layer obeys the sequence of $Al_{i-2} > Al_{i-1} > Al_i > Al_{bulk}$ (Table S6). Thus, the Al atoms at three Al layers near the interface are all subjected to tensile strain. For the Sc-alloyed interface (Fig. 6f), the Voronoi volume of the Sc atom obtains the maximum value. Combined with the increase of Voronoi volume of Al atoms, the Sc alloying can relieve the strain stress in the initial interface, which is beneficial to the interfacial stability and wettability. However, for the Ni-alloyed interface (Fig. 6g), the situation is the opposite. The Ni replacement causes the contrary compress strain into the Al(111)/TiB_2(0001) interface to weaken the interface performance. Combined with the alloying effects of Sc and Ni on the Al (001)/TiB_2(0001) interface, it can be found that the strain distribution of the initial interface is crucial to alloying effect. A similar alloying effect also can be found in grain boundaries with different orientations, such as Mg [28], Si [56], Mo [68].

When the Zn atoms are substituted in the Al(111)/TiB_2(0001) interface (Fig. 6h), the Voronoi volumes of both Zn and Al atoms show slight variation. Referring to the volume change in the Zn-alloyed Al (001)/TiB_2(0001) interface, it can be found that Zn alloying has a faint influence on the interfacial strain. According to the analogous atomic radius between the Zn and Al atoms (Table S4), it can be concluded that the alloying effect of Zn is also determined by the performance of the solute atom, which is similar to the Bi, Pb, Tl, and In elements in the Mg grain boundaries [21].

Overall, the Sc doping increases the charge accumulations and relieves the tensile strain in the Al(111)/TiB_2(0001) interface, which improves the interfacial stability and wettability. Similarly, the Ni alloying increases the charge accumulations and weakens the compressive strain in the Al(001)/TiB_2(0001) interface to enhance its performance. Thus, the alloying effects of Sc and Ni additions are determined by the interfacial structure. Besides, the Zn doping has less effect on the interfacial strain and charge density for both interfaces due to the similar electronegativity and atomic size with the Al atom. It means that the alloying effect of such elements is also determined by the performance of doping atoms. Therefore, the alloying effects on the Al/TiB_2 interfaces depend not only on the properties of solute atoms but also on the interfacial structure.

4. Conclusions

The alloying behaviors of Sc, Ni, and Zn at both Al(001)/TiB_2(0001) and Al(111)/TiB_2(0001) interfaces were explored via DFT calculation. The interfacial stability and wettability have been evaluated by the interface energy and work of adhesion. The alloying mechanism is analyzed by the charge density difference and Voronoi volume. The following conclusions are drawn:

(1) In the initial Al(001)/TiB_2(0001) and Al(111)/TiB_2(0001) interfaces, the interfacial Al atoms prefer to obey the center

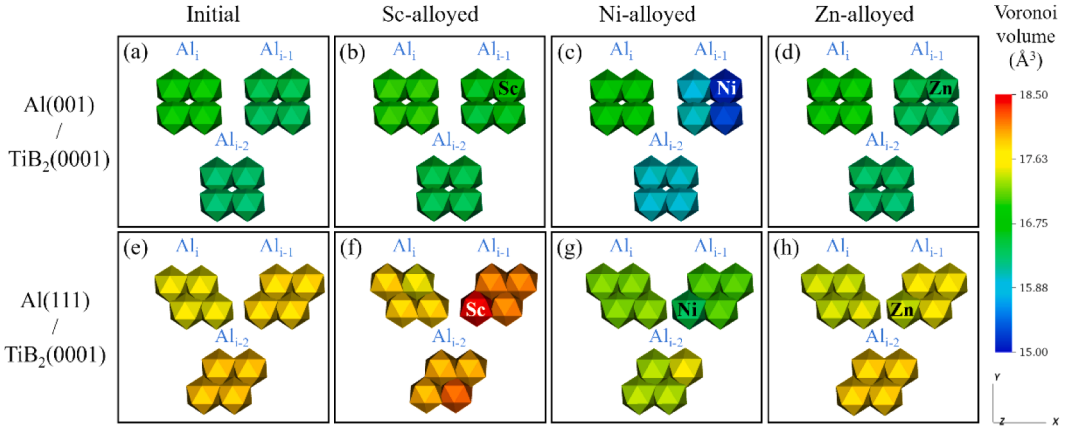

Fig. 6. Distributions map of Voronoi volumes of Al layers (i.e., Al_i, Al_{i-1}, Al_{i-2} layers) in Ti-center Al/TiB_2 interfaces without and with alloying atoms substitute at Al_{i-1} layer.

stacking sequence of the TiB_2 surface atoms. Moreover, the Ti terminated interfaces show higher thermodynamic stability.

(2) The additions of Sc, Ni, and Zn show opposite alloying effects on both Al/TiB_2 interfaces. For interfacial stability, the alloyed Al (001)/TiB_2(0001) interface follows the sequence of Ni > Zn > Sc, while it changes to the order of Sc > Zn > Ni on the alloying Al (111)/TiB_2(0001) interface. For interfacial wettability, only Sc- and Ni-alloyed Al(111)/TiB_2(0001) interfaces display a noticeable enhancement, while the others show a weak alteration. Thus, the interfacial orientation has an important influence on the alloying effect.

(3) The alloying mechanisms of Sc, Ni, and Zn additions are different. The Sc and Ni alloying mainly depend on the charge density distribution and strain distribution of the initial interface. It means that alloying effect of Sc and Ni is hinged on the interfacial structure. The Zn addition has a weak alloying effect due to the similar electronegativity and atomic size between Al and Zn atoms. Therefore, the alloying effects on the Al/TiB_2 interfaces are dependent not only on the properties of solute atoms but also on the interfacial orientation.

CRediT authorship contribution statement

Qian Wang: Conceptualization, Data curation, Formal analysis, Software, Writing – original draft. **Yuanyuan Li:** Formal analysis, Software, Writing – review & editing. **Zhe Chen:** Methodology, Writing – review & editing. **Mingliang Wang:** Conceptualization, Formal analysis, Funding acquisition, Writing – review & editing. **Hong Zhu:** Conceptualization, Formal analysis, Writing – review & editing. **Haowei Wang:** Supervision, Writing – review & editing.

Declaration of Competing Interest

On behalf of all authors, we declare that we have no financial and personal relationships with other people or organizations that can inappropriately influence our work, there is no professional or other personal interest of any nature or kind in any product, service and/or company that could be construed as influencing the position presented in, or the review of, the manuscript entitled, “Understanding alloying behaviors of Sc, Ni and Zn additions on Al/TiB2 interfaces based on interfacial characteristics and solute properties”.

Acknowledgments

This work is sponsored by the project funded by the National Natural Science Foundation of China (grant no. 52071207), by the National Key Research and Development Program of China (grant no. 2018YFB1106302), and the National Natural Science Foundation of China (grant no. 51821001).

Supplementary materials

Supplementary material associated with this article can be found, in the online version, at doi:10.1016/j.surfin.2021.101427.

References

[1] J. Moya, S. Lopezesteban, C. Pecharroman, The challenge of ceramic/metal microcomposites and nanocomposites, Prog. Mater Sci. 52 (2007) 1017–1090.
[2] S.B. Sinnott, E.C. Dickey, Ceramic/metal interface structures and their relationship to atomic-and mesoscale properties, Mater. Sci. Eng. R. 43 (2003) 1–59.
[3] L.L.J. Hashim, M.S.J. Hashmi, Particle distribution in cast metal matrix composites-Part I, J. Mater. Process. Technol. 123 (2002) 251–257.
[4] E. Saiz, R.M. Cannon, A.P. Tomsia, High-temperature wetting and the work of adhesion in metal/oxide systems, Annu. Rev. Mater. Res. 38 (2008) 197–226.
[5] S.Z. Han, E.A. Choi, S.H. Lim, S. Kim, J. Lee, Alloy design strategies to increase strength and its trade-offs together, Prog. Mater Sci. 117 (2021), 100720.
[6] W. Lv, L. Yan, X. Pang, H. Yang, L. Qiao, Y. Su, K. Gao, Study of the stability of α-Fe/MnS interfaces from first principles and experiment, Appl. Surf. Sci. 501 (2020), 144017.
[7] R.M.C. E.Saiz, A.P. Tomsia, Energetics, and atomic transport at liquid metal/Al_2O_3 interfaces, Acta Mater. 47 (1999) 4209–4220.
[8] H. Tong, F. Qiu, R. Zuo, P. Shen, X. Cong, J. Liu, H. Yang, Q. Jiang, The effect and mechanism of alloying elements on Al/SiC interfacial reaction in Al melt, Appl. Surf. Sci. 501 (2020), 144265.
[9] Y.M. Youssef, R.J. Dashwood, P.D. Lee, Effect of clustering on particle pushing and solidification behavior in TiB_2 reinforced aluminum PMMCs, Composites, Part A 36 (2005) 747–763.
[10] X. Zhang, P. Xu, M. Zhang, G. Liu, Z. Xu, J. Yang, H. Shao, G. Qiao, Improving the wettability of Ag/ZrB_2 system by Ti, Zr and Hf addition: an insight from first-principle calculations, Appl. Surf. Sci. 517 (2020), 146201.
[11] Q. Wang, Y. Li, S. Chen, X. Liu, Z. Chen, M. Wang, H. Zhu, H. Wang, Interface alloying design to improve the dispersion of TiB_2 nanoparticles in Al composites: a first-principles study, J. Phys. Chem. C 125 (2021) 5937–5946.
[12] L.F.C.F. Feng, Microstructures of in situ Al/TiB_2 MMCs prepared by a casting route, J. Mater. Sci. 35 (2000) 837–850.
[13] M. Wang, Y. Wang, J. Liu, Z. Chen, H. Chen, Y. Wu, F. Zhang, H. Wang, Effects of Zn content on microstructures and mechanical properties of in-situ TiB_2/Al-Zn-Mg-Cu composites subjected to hot extrusion, Mater. Sci. Eng. A 742 (2019) 364–372.
[14] I.K.L. Xi, R. Nowak, B. Korpała, G. Bruzda, N. Sobczak, N. Mattern, J. Eckert, High-temperature wetting and interfacial interaction between liquid Al and TiB_2 ceramic, J. Mater. Sci. 50 (2015) 2682–2690.
[15] I.K. Lixia Xi, Rafal Nowak, Grzegorz Bruzda, Natalia Sobczak, Wetting, reactivity, and phase formation at interfaces between Ni-Al melts and TiB_2 ultrahigh-temperature ceramic, J. Am. Ceram. Soc. 101 (2017) 1–8.
[16] L. Zhang, Q. Zheng, H. Jiang, J. Zhao, Interfacial energy between Al melt and TiB_2 particles and efficiency of TiB_2 particles to nucleate α-Al, Scr. Mater. 160 (2019) 25–28.
[17] H. Nakae, S. Wu, Behavior of ceramic particles at solid/liquid interface during solidification of metal matrix composites, Key Eng. Mater. 19A (1997) 503–510.
[18] J. Michael Humenik, William D. Kingery, Metal-ceramic interactions III, surface tension and wettability of metal-ceramic systems, J. Am. Ceram. Soc. 37 (1954) 18–23.
[19] W.Y. Wang, S.L. Shang, Y. Wang, F. Han, K.A. Darling, Y. Wu, X. Xie, O.N. Senkov, J. Li, X.D. Hui, K.A. Dahmen, P.K. Liaw, L.J. Kecskes, Z.K. Liu, Atomic and electronic basis for the serrations of refractory high-entropy alloys, NPJ Comput. Mater. 3 (2017) 1–10.
[20] C. Zou, J. Li, W.Y. Wang, Y. Zhang, D. Lin, R. Yuan, X. Wang, B. Tang, J. Wang, X. Gao, H. Kou, X. Hui, X. Zeng, M. Qian, H. Song, Z.-K. Liu, D. Xu, Integrating data mining and machine learning to discover high-strength ductile titanium alloys, Acta Mater. 202 (2021) 211–221.
[21] C. He, Z. Li, H. Chen, N. Wilson, J.F. Nie, Unusual solute segregation phenomenon incoherent twin boundaries, Nat. Commun. 12 (2021) 722.
[22] M.A. Gibson, C.A. Schuh, A survey of ab-initio calculations shows that segregation-induced grain boundary embrittlement is predicted by bond-breaking arguments, Scr. Mater. 113 (2016) 55–58.
[23] M.A. Gibson, C.A. Schuh, Segregation-induced changes in grain boundary cohesion and embrittlement in binary alloys, Acta Mater. 95 (2015) 145–155.
[24] J. Wang, M. Enomoto, C. Shang, First-principles study on the interfacial segregation at coherent Cu precipitate/Fe matrix interface, Scr. Mater. 185 (2020) 42–46.
[25] D. Zhao, Y. Li, Revealing the factors influencing grain boundary segregation of P, As in Si: insights from first-principles, Acta Mater. 168 (2019) 52–62.
[26] X. Gao, H. Wang, C. Ma, M. Lv, H. Ren, Segregation of alloying elements at the bcc-Fe/B_2-NiAl interface and the corresponding effects on the interfacial energy, Intermetallics 131 (2021), 107096.
[27] A.T. AlMotasem, T. Huminiuc, T. Polcar, Factors controlling segregation tendency of solute Ti, Ag and Ta into different symmetrical tilt grain boundaries of tungsten: First-principles and experimental study, Acta Mater. 211 (2021), 116868.
[28] T. Tsuru, H. Somekawa, D.C. Chrzan, Interfacial segregation and fracture in Mg-based binary alloys: experimental and first-principles perspective, Acta Mater. 151 (2018) 78–86.
[29] D. Shin, A. Shyam, S. Lee, Y. Yamamoto, J.A. Haynes, Solute segregation at the Al/θ′-Al_2Cu interface in Al-Cu alloys, Acta Mater. 141 (2017) 327–340.
[30] J.F. Nie, Y.M. Zhu, J.Z. Liu, X.Y. Fang, Periodic segregation of solute atoms in fully coherent twin boundaries, Science 340 (2013) 957–960.
[31] P.L. Schaffer, D.N. Miller, A.K. Dahle, Crystallography of engulfed and pushed TiB_2 particles in aluminum, Scr. Mater. 57 (2007) 1129–1132.
[32] Y. Tang, Z. Chen, A. Borbély, G. Ji, S.Y. Zhong, D. Schryvers, V. Ji, H.W. Wang, Quantitative study of particle size distribution in an in-situ grown Al-TiB_2 composite by synchrotron X-ray diffraction and electron microscopy, Mater. Charact. 102 (2015) 131–136.
[33] Y. Ma, A. Addad, G. Ji, M.-X. Zhang, W. Lefebvre, Z. Chen, V. Ji, Atomic-scale investigation of the interface precipitation in TiB_2 nanoparticles reinforced Al-Zn-Mg-Cu matrix composite, Acta Mater. 185 (2020) 287–299.
[34] Y. Han, Y. Dai, D. Shu, J. Wang, B. Sun, First-principles calculations on the stability of Al/TiB_2 interface, Appl. Phys. Lett. 89 (2006) 1441071–14410713.
[35] A.P.H. David Wearing, W.W. Xu, Peter D. Lee, Which wets TiB_2 inoculant particles: Al or Al_3Ti? J. Alloys Compd. 664 (2016) 460–468.
[36] C. Deng, B. Xu, P. Wu, Q. Li, Stability of the Al/TiB_2 interface and doping effects of Mg/Si, Appl. Surf. Sci. 425 (2017) 639–645.

[37] J. Xue, Y. Han, J.B. Lei, J. Wang, B. Sun, CeO_2 induced dispersive distribution of TiB_2 particles in in-situ TiB_2/Al composite, Mater. Sci. Technol. 30 (2013) 871–875.
[38] R.P. Feynman, Forces in molecules, Phys. Rev. 56 (1939) 340–343.
[39] P.E. Blochl, Projector augmented-wave method, Phys. Rev. B 50 (1994) 17953–17979.
[40] G. Kresse, D. Joubert, From ultrasoft pseudopotentials to the projector augmented wave method, Phys. Rev. B 59 (1999) 1758–1775.
[41] K.B. John, P. Perdew, Matthias Ernzerhof, Generalized gradient approximation made simple, Phys. Rev. Lett. 77 (1996) 3865–3868.
[42] G. Pilania, B.J. Thijsse, R.G. Hoagland, I. Lazic, S.M. Valone, X.Y. Liu, Revisiting the Al/Al_2O_3 interface: coherent interfaces and misfit accommodation, Sci. Rep. 4 (2014) 4485.
[43] Y.X. Wu, X.Y. Li, Y.M. Wang, First-principles study of the influence of lattice misfit on the segregation behaviors of hydrogen and boron in the Ni-Ni_3Al system, Acta Mater. 55 (2007) 4845–4852.
[44] Y.F. Li, B. Xiao, G.L. Wang, L. Sun, Q.L. Zheng, Z.W. Liu, Y.M. Gao, Revealing the novel fracture mechanism of the interfaces of TiB_2/Fe composite from a first-principles investigation, Acta Mater. 156 (2018) 228–244.
[45] H.Y. Xu, H.Y. Wang, M. Zha, C. Wang, Z.Z. Yang, Q.C. Jiang, Effects of Ti, Si, Mg and Cu additions on interfacial properties and electronic structure of Al(111)/4H-SiC(0001) interface: a first-principles study, Appl. Surf. Sci. 437 (2018) 103–109.
[46] Z.J. Wang, S. Liu, Z.X. Qiu, H.Y. Sun, W.C. Liu, First-principles calculations on the interface of the Al/TiC aluminum matrix composites, Appl. Surf. Sci. 505 (2020), 144502.
[47] X.-G. Wang, W. Weiss, S.K. Shaikhutdinov, M. Ritter, M. Petersen, F. Wagner, R. Schlögl, M. Scheffler, The hematite (α-Fe_2O_3)(0001) surface: evidence for domains of distinct chemistry, Phys. Rev. Lett. 81 (1998) 1038.
[48] W. Zhang, J. Smith, Nonstoichiometric interfaces and Al_2O_3 adhesion with Al and Ag, Phys. Rev. Lett. 85 (2000) 3225.
[49] Q. Wang, C. Liu, R. Yao, H. Zhu, X. Liu, M. Wang, Z. Chen, H. Wang, First-principles study on the stability and work function of low-index surfaces of TiB_2, Comput. Mater. Sci. 172 (2020), 109356.
[50] W. Zhao, Z. Sun, S. Gong, Vacancy mediated alloying strengthening effects on γ/γ′ interface of Ni-based single crystal superalloys: a first-principles study, Acta Mater. 135 (2017) 25–34.
[51] W. Zhang, J.R. Smith, X.G. Wang, A.G. Evans, Influence of sulfur on the adhesion of the nickel/alumina interface, Phys. Rev. B 67 (2003) 2454141–24541412.
[52] S. Chen, Y. Pan, Noble metal interlayer-doping enhances the catalytic activity of 2H–MoS_2 from first-principles investigations, Int. J. Hydrogen Energy 46 (2021) 21040–21049.
[53] S. Chen, Y. Pan, Influence of Group III and IV elements on the hydrogen evolution reaction of MoS2 disulfide, J.Phys. Chem. C 125 (2021) 11848–11856.
[54] Y. Pan, The influence of Ag and Cu on the electronic and optical properties of ZrO from first-principles calculations, Mater. Sci. Semicond. Process. 135 (2021), 106084.
[55] Y. Pan, E. Yu, First-principles investigation of electronic and optical properties of H-doped FeS_2, Int. J. Energy Res. 45 (2021) 11284–11293.
[56] R. Maji, E. Luppi, N. Capron, E. Degoli, Ab initio study of oxygen segregation in silicon grain boundaries: the role of strain and vacancies, Acta Mater. 204 (2021), 116477.
[57] Y.Q. Guo, S.H. Zhang, I.J. Beyerlein, D. Legut, S.L. Shang, Z.K. Liu, R.F. Zhang, Synergetic effects of solute and strain in biocompatible Zn-based and Mg-based alloys, Acta Mater. 181 (2019) 423–438.
[58] R. Mahjoub, K.J. Laws, N. Stanford, M. Ferry, General trends between solute segregation tendency and grain boundary character in aluminum—an ab into study, Acta Mater. 158 (2018) 257–268.
[59] X.Y. Xu, H.Y. Wang, M. Zha, C. Wang, Z.Z. Yang, Q.C. Jiang, Effects of Ti, Si, Mg and Cu additions on interfacial properties and electronic structure of Al(111)/4H-SiC(0001) interface: a first-principles study, Appl. Surf. Sci. 437 (2018) 103–109.
[60] Y. Pan, The influence of N-vacancy on the electronic and optical properties of bulk InN nitrides, Mater. Sci. Eng. B 271 (2021), 115265.
[61] Y. Pan, E. Yu, D. Wang, H. Deng, Sulfur vacancy enhances the electronic and optical properties of FeS_2 as the high-performance electrode material, J. Alloys Compd. 858 (2021), 157662.
[62] Y. Pan, J. Zhang, Influence of noble metals on the electronic and optical properties of the monoclinic ZrO_2: a first-principles study, Vacuum 187 (2021), 110112.
[63] J. Liu, E. Tennessen, J. Miao, Y. Huang, J.M. Rondinelli, H. Heinz, Understanding chemical bonding in alloys and the representation in atomistic simulations, J. Phys. Chem. C 122 (2018) 14996–15009.
[64] D. Chen, C. Xia, X. Liu, Y. Wu, M.J.M. Wang, The effect of alloying elements on the structural stability, and mechanical and electronic properties of Al_3Sc: a first-principles study, Materials 12 (2019) 1539.
[65] S.P. Sun, X.P. Li, H.J. Wang, H.F. Jiang, W.N. Lei, Y. Jiang, D.Q. Yi, First-principles investigations on the electronic properties and stabilities of low-index surfaces of $L1_2$-Al_3Sc intermetallic, Appl. Surf. Sci. 288 (2014) 609–618.
[66] U. Saikia, M.B. Sahariah, C. Gonzalez, R. Pandey, Vacancy assisted He-interstitial clustering and their elemental interaction at the fcc-bcc semicoherent metallic interface, Sci. Rep. 8 (2018) 3844.
[67] C.H. Rycroft, VORO++: a three-dimensional Voronoi cell library in C++, Chaos 19 (2009), 041111.
[68] R. Tran, Z. Xu, N. Zhou, B. Radhakrishnan, J. Luo, S.P. Ong, Computational study of metallic dopant segregation and embrittlement at molybdenum grain boundaries, Acta Mater. 117 (2016) 91–99.